NANO LETTERS

Letter

pubs.acs.org/NanoLett

Biphase Stratification Approach to Three-Dimensional Dendritic Biodegradable Mesoporous Silica Nanospheres

Dengke Shen,[⊥] Jianping Yang,[⊥] Xiaomin Li, Lei Zhou, Renyuan Zhang, Wei Li, Lei Chen, Rui Wang, Fan Zhang,* and Dongyuan Zhao*

Department of Chemistry, Shanghai Key Laboratory of Molecular Catalysis and Innovative Materials, State Key Laboratory of Molecular Engineering of Polymers and Laboratory of Advanced Materials, Fudan University, Shanghai 200433, People's Republic of China

Supporting Information

ABSTRACT: A kind of novel uniform monodispersed three-dimensional dendritic mesoporous silica nanospheres (3D-dendritic MSNSs) has been successfully synthesized for the first time. The 3D-dendritic MSNSs can have hierarchical mesostructure with multigenerational, tunable center-radial, and dendritic mesopore channels. The synthesis was carried out in the heterogeneous oil−water biphase stratification reaction system, which allowed the self-assembly of reactants taking place in the oil−water interface for one-pot continuous interfacial growth. The average pore size of each generation for the 3D-dendritic MSNSs can be adjusted from 2.8 to 13 nm independently, which can be controlled by the varied hydrophobic solvents and concentration of silica source in the upper oil phase. The thickness of each generation can be tuned from ∼5 to 180 nm as desired, which can be controlled by the reaction time and amount of silica source. The biphase stratification approach can also be used to prepare other core−shell and functional mesoporous materials such as Au nanoparticle@3D-dendritic MSNS and Ag nanocube@3D-dendritic MSNS composites. The 3D-dendritic MSNSs show their unique advantage for protein loading and releasing due to their tunable large pore sizes and smart hierarchical mesostructures. The maximum loading capacity of bovine β-lactoglobulin with 3D-dendritic MSNSs can reach as high as 62.1 wt % due to their large pore volume, and the simulated protein releasing process can be tuned from 24 to 96 h by flexible mesostructures. More importantly, the releasing rates are partly dependent on the hierarchical biodegradation, because the 3D-dendritic MSNSs with larger pore sizes have faster simulated biodegradation rates in simulated body fluid. The most rapid simulated biodegradation can be finished entirely in 24 h, which has been greatly shortened than two weeks for the mesoporous silica reported previously. As the inorganic mesoporous materials, 3D-dendritic MSNSs show excellent biocompatibility, and it would have a hopeful prospect in the clinical applications.

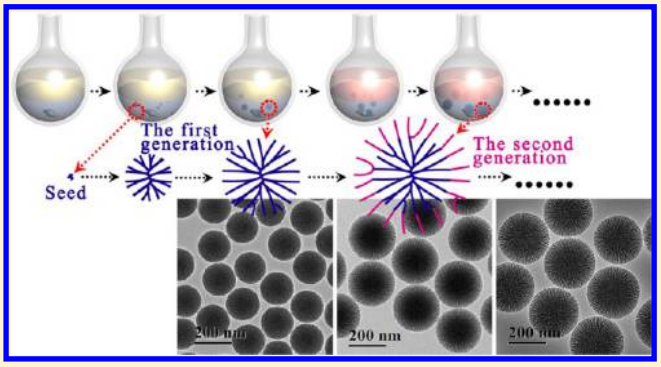

KEYWORDS: *Mesoporous silica, interfacial synthesis, biodegradation, nanospheres, assembly, emulsion*

Mesoporous silica-based materials have undergone a spectacular evolution during the last decades with great contributions to the developments in areas ranging from separation, adsorption, catalysis, and biomedicine due to the high surface area and large pore volume.[1−8] Particularly, in the application of nanodrug delivery systems, ordered mesoporous silica nanoparticles have become an alternative to traditional organic emulsions or liposomes due to the advantages of inorganic materials, such as its rigid mesostructured framework,[9] and high stability to varied temperature and organic solvents.[10] Unfortunately, drug delivery applications using mesoporous silica are usually limited to the small molecule drugs (molecular size <2 nm)[11,12] because it is still a large challenge to synthesize uniform monodispersed mesoporous silica nanoparticles with uniform large pores (pore size >5 nm) suitable for in vivo bioapplication.[13−18] However, it is important to note that macromolecular drugs (molecular size >2 nm) such as proteins and peptides are increasingly recognized as potential leading for the development of new therapeutics for a variety of human ailments.[19,20] Therefore, it is desirable to fabricate colloidal mesoporous silica nanoparticles with pore sizes from 5 to 13 nm to match that of regular protein drugs.[21] An inspiration from dendrimer organic compounds, which is a kind of polymers with multigenerational hierarchical structure,[22−24] herein, novel silica-based nanocarriers with dendritic hierarchical mesostructure were fabricated as designed with dendritic center-radial oriented large mesopores. These novel inorganic nanocarriers would be hopeful to improve the controllability of protein loading and release.

Received: November 20, 2013
Revised: January 16, 2014
Published: January 27, 2014

Furthermore, biodegradability is still a roadblock for the biomedical applications of inorganic materials.[25−29] Previous reports have revealed that the whole degradation process of conventional mesoporous silica nanospheres would last one or two weeks depending on the particle diameters and mesopore size.[30,31] In vivo excretion data showed that the entire clearance time of these nanoparticles could be over 4 weeks, and their accumulation in liver and spleen was bound to cause tissue damage.[32] In order to seek faster degradation rates in simulated body fluid, colloidal mesoporous silica nanoparticles with a large pores, thin pore wall, and low cross-linking degree are much desired.

Soft-templating approach is one of the current most useful synthetic methods for the ordered mesoporous silicas via surfactant molecular self-assembly.[33] Several methods have been reported, including the hydrothermal method in aqueous media[34−36] and solvent evaporation-induced self-assembly (EISA) in nonaqueous media.[37] It has indicated that the soft-templating approach usually needs a homogeneous reaction system, whether the soft templates are micelles assembled with surfactants or nanoemulsions constituted of surfactants and oil drops.[30,38−43] To the best of our knowledge, there were no reports about the preparation of uniform monodispersed mesoporous silica nanospheres with large center-radial pore channels in oil−water biphase stratification reaction system, which is a heterogeneous reaction occurred in the macroscopic interface.

Herein, we demonstrate a novel kind of "inorganic dendrimer", three-dimensional dendritic mesoporous silica nanospheres (3D-dendritic MSNSs) with a tunable size and controlled center-radial mesostructure, which can be grown generationally and hierarchically as the regular organic dendrimer. The 3D-dendritic MSNSs were synthesized by a novel oil−water biphase stratification approach for the first time. The average pore size of each generation can be adjusted from 2.8 to 13 nm independently, and the thickness can be tuned from ∼5 to 180 nm as desired. Most importantly, we found that the 3D-dendritic MSNSs could be biodegraded with a very rapid rate in the simulated body fluid. The fastest simulated biodegradation can be finished entirely in 24 h, which is greatly shortened than the two weeks for mesoporous silica reported previously.

The 3D-dendritic MSNSs can be prepared in a heterogeneous oil−water biphase stratification reaction system (Scheme 1 and Figure S1 in Supporting Information). The biphase stratification approach allows the reaction to take place in the interface, and it is convenient to control the assembly on the interface via changing or adding reactants in each phase without disturbing the interface. The upper oil phase is a tetraethyl orthosilicate (TEOS) solution with hydrophobic organic solvent, while the lower aqueous phase is an aqueous solution combined by cationic cetyltrimethylammonium chloride (CTAC) as a template and organic base triethanolamine (TEA) as a catalyst. The dendritic hierarchical mesostructure with several generations can be achieved with a one-pot continuous interfacial growth route, and the pore size can be controlled by changing different hydrophobic solvents.

The transmission electron microscope (TEM) and scanning electron microscope (SEM) images of the typical 3D-dendritic MSNSs with three generations prepared via the biphase stratification continuous growth approach are shown in Figure 1. The first generation 3D-dendritic MSNSs are highly uniform mesoporous nanospheres with a mean particle size of ∼180 nm

Scheme 1. Synthesis Process of the 3D-Dendritic MSNSs and Mechanism of Interfacial Growth[a]

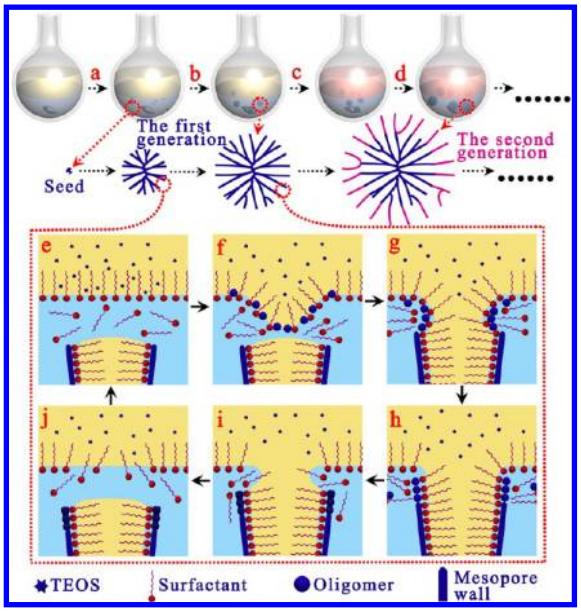

[a](a) Nucleation process of the 3D-dendritic MSNSs; (b) growth process of the first generation of the 3D-dendritic MSNSs; (c) changing the upper oil phase; (d) growth process of the second generation of the 3D-dendritic MSNSs; (e−h) the mechanism of one single mesopore-channel growth with swelling.

(Figure 1a,d). The center-radial mesopore channels (∼2.8 nm) can be clearly observed in the TEM image (Supporting Information Figure S2a). A single scattering peak at ∼1.23 nm^{-1} in small-angle X-ray scattering (SAXS) pattern can be observed, suggesting a uniform mesostructure of the first generation nanospheres (Figure 1g, black line). According to the nitrogen adsorption−desorption isotherms, a capillary condensation step at around $0.2 < P/P_0 < 0.4$ is obviously observed, providing a clear evidence for their narrow pore size distribution (Figure 1h, black line). The BET surface area is measured to be ∼598 $m^2\ g^{-1}$, and the total pore volume is found to be ∼0.571 $cm^3\ g^{-1}$. Using the density functional theory (DFT) method, the pore size of the first-generation 3D-dendritic MSNSs is estimated to be about 2.8 nm in diameter (Figure 1i, black line). TEM image shows that the 3D-dendritic MSNSs with two generations have the core−shell structure, and their average particle size is ∼250 nm (Figure 1b). Compared with the first generation with the thickness of ∼180 nm, the second generation 3D-dendritic MSNSs have the thickness of ∼35 nm as the shell. In TEM image, the mesopore size of the shells for the second generation the 3D-dendritic MSNSs is found to be ∼5.5 nm (Supporting Information Figure S2b), which is obviously larger than that of the first generation nanospheres. The SEM image of the 3D-dendritic MSNSs with two generations (Figure 1e) shows the irregular craters on the surface of the nanospheres, revealing the opening mesochannels. Two scattering peaks at ∼1.23 and ∼0.83 nm^{-1} are observed in the SAXS pattern of the two generation 3D-dendritic MSNS products (Figure 1g, red line). The scattering peak at ∼1.23 nm^{-1} is the same with the one of first generation nanospheres, and another peak at ∼0.83 nm^{-1} is due to the second generation. It indicates the existence of a hierarchical uniform mesostructure in the two-generation products. The capillary condensation step expands to $0.2 < P/P_0 < 0.7$ in the

dx.doi.org/10.1021/nl404316v | Nano Lett. 2014, 14, 923−932

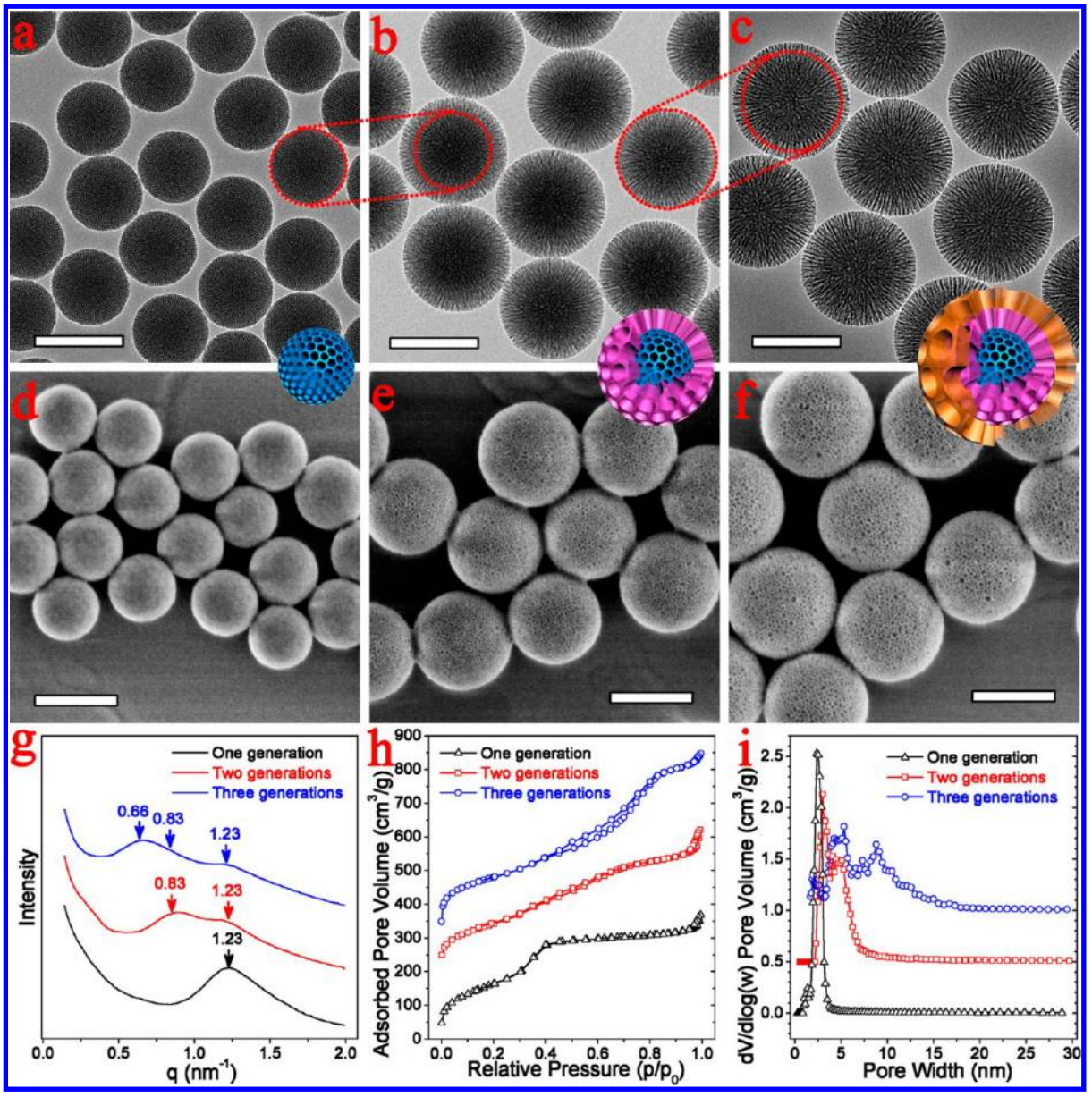

Figure 1. TEM (a–c) and SEM (d–f) images of the extracted 3D-dendritic MSNSs with one (a,d), two (b,e), and three generations (c,f) prepared via the biphase stratification approach; SAXS patterns (g) of the extracted 3D-dendritic MSNSs with one (black), two (red), and three generations (blue); nitrogen adsorption–desorption isotherms (h) and pore size distribution (i) of the extracted 3D-dendritic MSNSs with one (black), two (red), and three generations (blue). All the 3D-dendritic MSNS products were extracted by NH_4NO_3-ethanol three times to remove the surfactant templates. All scalebars in TEM and SEM images are 200 nm.

N_2 sorption isotherms, and the hysteresis loops appear in $0.4 < P/P_0 < 0.7$ (Figure 1h, red line), implying a bimodal mesopore. The BET surface area and total pore volume are calculated to be about 518 $m^2\ g^{-1}$ and 0.689 $cm^3\ g^{-1}$, respectively. The pore size distribution reveals the bimodal mesopores at the mean values of ~2.8 and 5.5 nm (Figure 1i, red line), demonstrating the close connectivity and continuous pore channels between the first generation and the second generation. The 3D-dendritic MSNSs with three generations keep their highly uniform particle size, which is about 280 nm (Figure 1c). Compared with the two-generation products, the third generation 3D-dendritic MSNSs have the shell thickness of ~15 nm and the larger pore size of ~10 nm (Supporting Information Figure S2c). These particles are full of craters on the surface (Figure 1f), also revealing an opening state of the mesopore channels on the third-generation shells. The SAXS pattern of the three-generation 3D-dendritic MSNSs show three scattering peaks at ~0.66, 0.83, and 1.23 nm^{-1}, indicating uniform mesostructures with three different cell parameters and pore sizes (Figure 1g, blue line). It further suggests a hierarchically mesoporous structure. The BET surface area and total pore volume are measured to be ~647 $m^2\ g^{-1}$ and 0.896 $cm^3\ g^{-1}$, respectively. An evident capillary condensation step and hysteresis loop can be observed at the relative pressure around $0.2 < P/P_0 < 0.8$ in the N_2 sorption isotherms, suggesting the wide pore size distributions (Figure 1h, blue line). Their tripartite sizes of the uniform mesopores are revealed by the DFT method, including a small pore with the size of ~2.8 nm for the first generation 3D-dendritic MSNSs, a middle mesopore of ~5.5 nm for the second generation and a

dx.doi.org/10.1021/nl404316v | Nano Lett. 2014, 14, 923–932

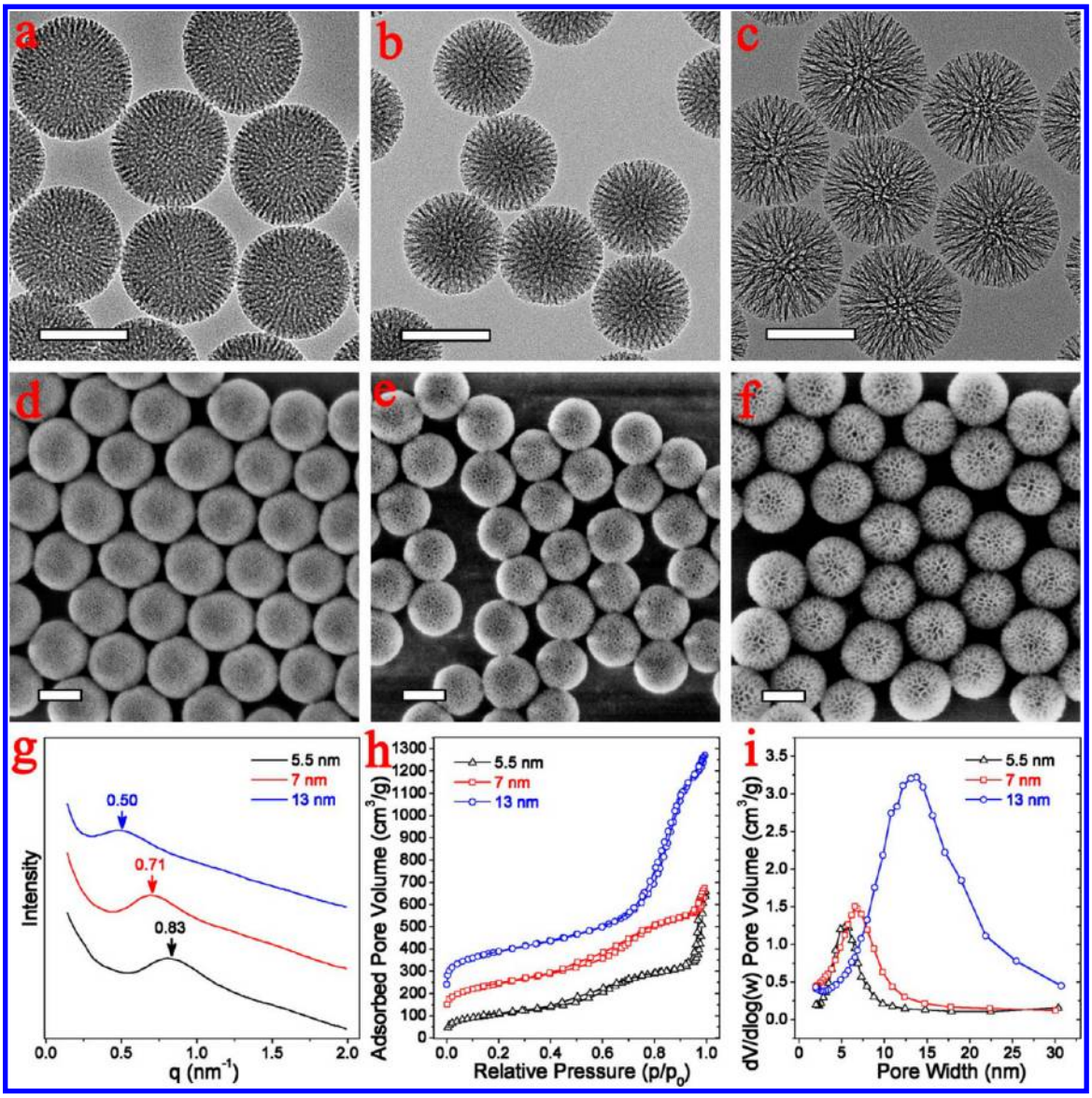

Figure 2. TEM (a–c), SEM (d–f) images, SAXS patterns (g), and nitrogen adsorption–desorption isotherms (h) and pore size distribution (i) of the single-generation 3D-dendritic MSNSs with a mesopore size of ~5.5 nm (a, d, and black color lines), ~7 nm (b, e, and red color lines), and ~13 nm (c, f, and blue color lines) via our biphase stratification approach with the different oil phase parameters. All the 3D-dendritic MSNS products were extracted by NH_4NO_3-ethanol for three times to remove the surfactant templates. All scalebars in TEM and SEM images are 100 nm.

large pore of ~10 nm for the third generation (Figure 1i, blue line). In addition, the colored photonic crystal films constituted of the 3D-dendritic MSNSs can be formed at the glass surface by the EISA approach (Supporting Information Figure S1), indicating that the highly uniformity and monodispersity of the nanospheres are achieved via our biphase stratification synthesis approach.

The preparation of the 3D-dendritic MSNSs is a convenient one-pot synthesis process, and the size of the mesopores highly depends on the hydrophobic organic solvent of the upper oil phase in heterogeneous oil–water biphase stratification reaction system (shown in Scheme 1 and Supporting Information Figure S2). With the single generation 3D-dendritic MSNSs synthesis as an example, when the solution of (20 v/v %) TEOS in 1-octadecene is used as the upper oil phase, the pore size of ~2.8 nm in diameter can be realized (Figure 1a). It has the similar pore size for the products from CATC as a template in homogeneous aqueous media.[44] However, when the solvent is replaced with decahydronaphthalene, the 3D-dendritic MSNSs with the mesopore size of ~5.5 nm can be achieved (Figure 2a). It reveals that there is a swelling behavior in decahydronaphthalene–water biphase stratification reaction system. Meanwhile, cyclohexane with 10 v/v % TEOS in upper oil-phase leads to a more effective swelling behavior, and the mesopore size can be increased to ~10 nm (Figure 3b). These results suggest that the organic molecules play a key role in swelling behavior, and the different molecular sizes and hydrophobicity of them lead to the mesopores with different pore sizes.

On the other hand, the concentration of TEOS in the hydrophobic organic solvent is another factor to adjust the pore sizes in heterogeneous oil–water biphase stratification reaction system. The 3D-dendritic MSNSs with a pore size of ~10 nm can be obtained with 10 v/v % of TEOS in cyclohexane solution. The pore size of ~7 nm can be achieved with a 20 v/v % TEOS cyclohexane solution (Figure 2b,e), while a 5 v/v %

dx.doi.org/10.1021/nl404316v | Nano Lett. 2014, 14, 923–932

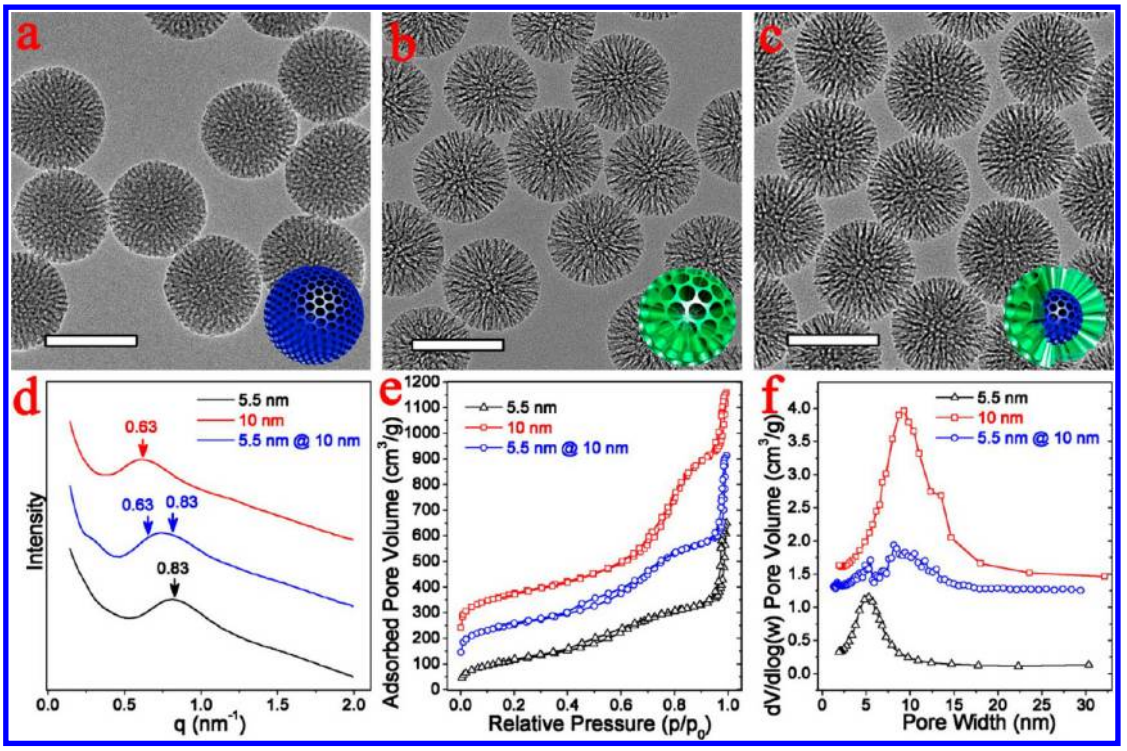

Figure 3. TEM images (a–c), SAXS patterns (d), nitrogen adsorption–desorption isotherms (e), and pore size distribution (f) of the 3D-dendritic MSNSs with different pore size of ~5.5 nm (a, and black lines in d–f), ~10 nm (b, and red lines in d–f), and two-generation 3D-dendritic MSNSs with a bimodal mesopore size of ~5.5 nm inside and ~10 nm outside (c, and blue lines in d–f). All the 3D-dendritic MSNS products were extracted by NH_4NO_3-ethanol three times to remove the surfactant templates. All scalebars in TEM images are 100 nm.

TEOS cyclohexane solution leads to a pore size of ~13 nm (Figure 2c,f). Simultaneously, the pore volumes of the 3D-dendritic MSNS products are found to become larger with bigger pore sizes (Table 1). It suggests that reduction of the

Table 1. Synthesis Conditions of the 3D-Dendritic MSNS Products via Biphase Stratification Approach[a]

hydrophobic organic solvent	concentration of TEOS (v/v %)	mean size of pores (nm)	BET surface area (m^2 g^{-1})	volume of pores (cm^3 g^{-1})
1-octadecene	20	2.8	598	0.571
decahydronaphthalene	20	5.5	416	0.873
cyclohexane	20	7.0	523	0.889
cyclohexane	10	10	632	1.419
cyclohexane	5	13	681	1.656

[a]All the 3D-dendritic MSNS products were prepared with different upper oil phases but the same bottom aqueous phase as 10 wt % CTAC and 0.3 wt % TEA water solution at 60 °C for 12 h. All the 3D-dendritic MSNS products were extracted by NH_4NO_3-ethanol three times to remove the surfactant templates. All the pore sizes of the 3D-dendritic MSNS products were determined from the adsorption branch on the basis of the BJH model.

TEOS concentration of the silica source leads to assembly of the mesopores with larger sizes and volumes, which is related with the volume of emulsion involved by more hydrophibic organic molecules and less hydrophilic silicate oligomers. The experimental parameters and the corresponding 3D-dendritic MSNS products with different pore sizes are shown in Table 1.

Via our biphase stratification approach, not only can the pore size of the 3D-dendritic MSNSs be controlled but also the particle size can be tuned as desired. The 3D-dendritic MSNS products with a pore size of ~5.5 nm can be grown continuously with a particle size of ~80 nm at the reaction time for 8 h (Figure 4g) to 130 nm for 16 h (Figure 3a), and subsequently to 160 nm for 24 h (Figure 2a). In order to further illustrate the reaction process of the 3D-dendritic MSNSs, the synthesis of the single generation products with a pore size of ~7 nm were selected as the another example with meticulous monitoring. According to the TEM images of the products with different reaction time, the nanoparticles begin to appear with a particle size of ~45 nm after 2 h reaction, and grow to a particle size of ~75, ~90, ~111, ~124, and ~136 nm at the reaction time of 3, 4, 6, 8, and 12 h, respectively (Supporting Information Figure S4a–e and Figure 2b). It reveals that a nucleation-growth process occurs in the preparation of the 3D-dendritic MSNSs. The growth rate is found to become more and more slowly as the nanospheres growing up (Supporting Information Figure S4f), and the maximal thickness of each generation of the 3D-dendritic MSNSs is considered to be tuned within ~180 nm in a one-pot reaction. It also has been demonstrated that the 3D-dendritic MSNSs can be grown to larger particle size with the same pore size if the number of the nanoparticles is reduced, while the concentration of silica source and organic amine is maintained by continuous adding. On the other hand, the particle size of the 3D-dendritic MSNSs can be affected obviously by the reaction temperature. The synthesis of the single generation products with a pore size of ~7 nm were selected as the example with different reaction temperature, the particle size of the 3D-dendritic MSNSs can be increased from 75 to 145 nm when the temperature was increased from 45 to 75 °C, and the pore size of them maintained to be ~7 nm (Supporting Information Figure S10 and Figure 2b,e).

dx.doi.org/10.1021/nl404316v | Nano Lett. 2014, 14, 923–932

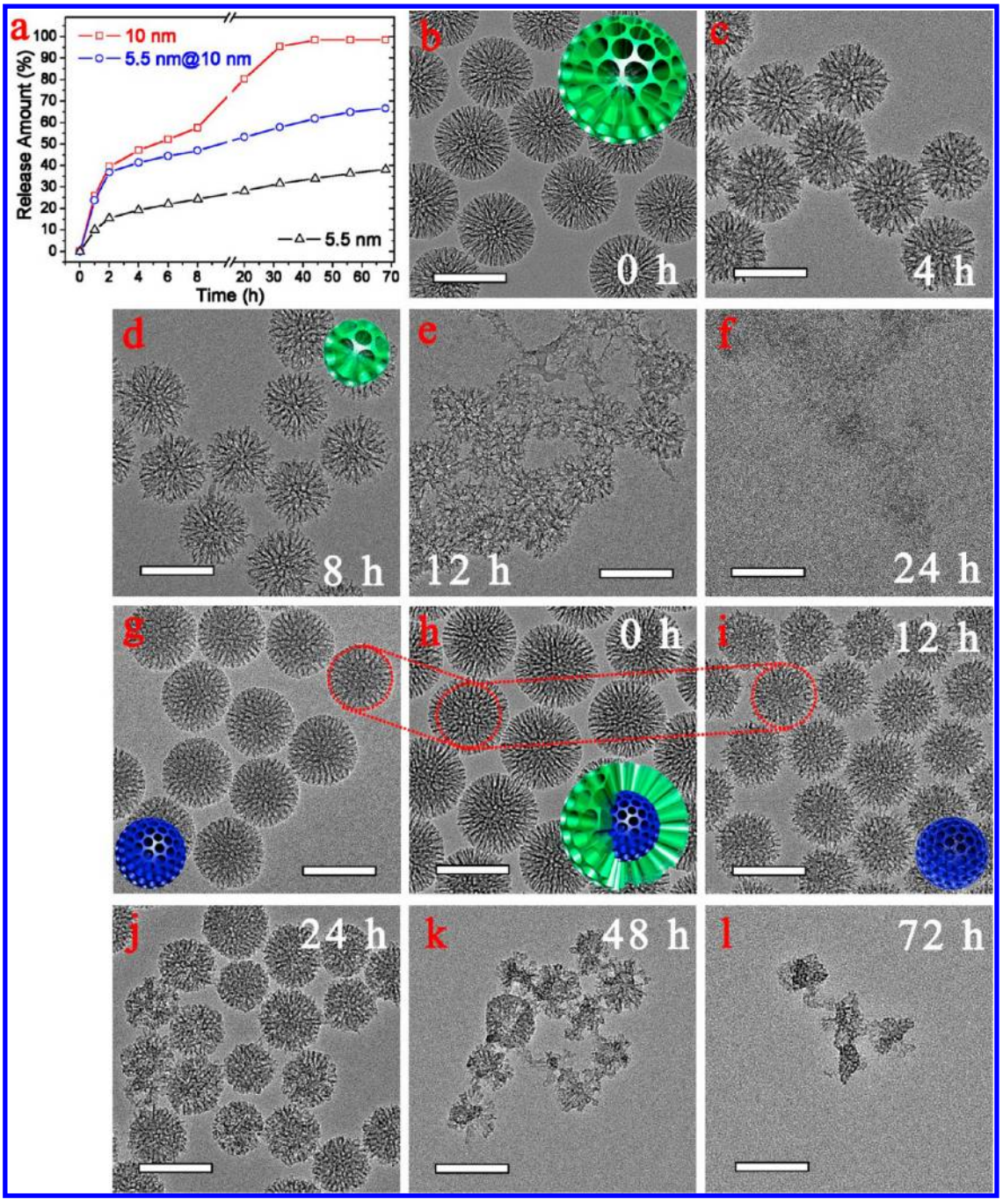

Figure 4. Protein release curves (a) of the 3D-dendritic MSNSs nanocarriers in Krebs solution at 37 °C and TEM images of the 3D-dendritic MSNSs nanocarriers (b–l) at different degradation intervals: the 3D-dendritic MSNS-10 nanocarriers with a large pore size of ~10 nm at (b) 0 h, (c) 4 h, (d) 8 h, (e) 12 h and (f) 24 h; the two-generation 3D-dendritic MSNS-5.5@10 nanocarriers with a hierarchical core–shell mesoporous structure and a small pore inside of 5.5 nm in size and a large pore outside of 10 nm, (g) the first-generation of 3D-dendritic MSNS-5.5@10 as the intermediate products, two-generations 3D-dendritic MSNS products at (h) 0 h, (i) 12 h, (j) 24 h, (k) 48 h, (l) 72 h. The loading capacity of corresponding 3D-dendritic MSNSs is set as 100% to calculate the release amount (%) in the protein release curves. All scalebars in TEM images are 100 nm.

In addition, the pore sizes can be well controlled in the desired generation for the 3D-dendritic MSNSs by changing the upper oil phase during different generation fabrication process as described above (Scheme 1c). The large pore size of ~10 nm in the second generation shells can be realized by changing 10 v/v % TEOS cyclohexane solution as the upper oil phase after the preparation of the first generation 3D-dendritic MSNSs, while the first generation nanospheres keep the pore size of ~5.5 nm due to using 20 v/v % TEOS decahydronaphthalene solution in the synthesis process (Figure 3c). Another kind of products with a large pore of ~10 nm in the first generation 3D-dendritic MSNSs and small pores of ~2.8 nm in the second generation can also be synthesized successfully (shown in Supporting Information Figure S3) by changing TEOS solution in reverse: first 10 v/v % TEOS cyclohexane solution, then 20 v/v % TEOS in the upper phase of organic solvent 1-octadecene.

dx.doi.org/10.1021/nl404316v | *Nano Lett.* 2014, 14, 923–932

Furthermore, it is found that the 3D-dendritic silica mesopore channels can be nucleated and grown on the surface of the gold nanoparticles. If the gold nanoparticles with a particle size of ~25 nm prepared according to the sodium citrate reduction method reported previously[45] are added in the aqueous phase of the bottom layer at the beginning of the reaction (Supporting Information Figure S5a), a core−shell Au@3D-dendritic MSNS structure can be obtained. It clearly indicates that the nucleation and growth of 3D-dendritic MSNSs on the heterogeneous surface of the Au nanoparticles are prior to the homogeneous one in the aqueous solution. Similarly, when the silver nanocubes with a particle size of ~40 nm prepared according to the NaHS-mediated polyol synthesis method reported previously[46,47] are added in the bottom aqueous phase and used as a core, the uniform core−shell Ag@3D-dendritic MSNS can also be achieved by the similar condition. Interestingly, the morphology of the core−shell nanoparticles is inclined to grow spherically (Supporting Information Figure S5b), which may be related to lowering the surface energy. These results clearly indicate that the biphase stratification approach can be expanded as a coating method for the preparation of other core−shell and functional mesoporous materials.

All results above reveal that the upper oil phase plays the key role in the preparation of the 3D-dendritic MSNSs. The hydrophobic organic solvent not only provides a storage medium for the silica resource (TEOS) but also interacts and assembles with the surfactant molecules on the interface to form oil@water emulsion micelles, which serve as a mesoscaled template to generate the ordered mesoporous silica structure with controlled pore diameters, particle sizes, and generation. Compared to the regular reactions in homogeneous system with the similar aqueous parameters,[48,49] it costs much more time in the formation of the 3D-dendritic MSNSs via the biphase stratification approach due to the slow diffusion and hydrolysis rates of silicates from the oil phase to aqueous phase and on the interface. It allows controlling the assembly and growth of the silica mesostructures. On the basis of the above results, we proposed a novel interfacial emulsion, "funneling" gradient assembly and growth process as shown in Scheme 1. The formation of the 3D-dendritic mesoporous silica nanospherical structures in the biphase stratification reaction system undergoes a complex process including interfacial emulsion to form oil@water hemimicelles, exclusive composite micelles on the solid nuclei, "funneling" gradient assembly, and growth of the mesostructures (Scheme 1e−h).

At first, due to the gravity and hydrophilic/hydrophobic interaction an oil@water hemiemulsion micelles with interfacial curvature can be induced by the surfactant assembled with hydrophobic organic solvent at the interface because a shear force from stirring.[50] Meanwhile, the silica source TEOS in the upper organic solvent gradually diffuses to the oil−water interface to hydrolyze and polymerize to form the silicate oligomers, which are continuously arranged at the hydrophilic zone of the curving interface of the hemimicelles due to their hydrophilic Si−OH groups (Scheme 1f). The silicate oligomers can further go into the aqueous phase to trigger the nucleation process when they reach the critical nucleation concentration (Scheme 1a). With the continuous and gentle stirring for the aqueous solution, the silicate/surfactant/oil composite nanoseeds can move randomly in aqueous phase and reach the interface and contact the curvature emulsion micelles containing oligomers to realize further growing and assembling with the "funneling" curvature (Scheme 1g). Then the silicate oligomers are further polymerized and condensed to form neonatal pore walls with the hemiemulsion as a template (Scheme 1h,i) then enter into the aqueous phase. The processes of interfacial emulsion, assembly, condensation, and "funneling" gradient growth can be continued circularly, since the nanoseeds (silicate/surfactant/oil composites) get in touch with the interface repeatedly via their free movement by the stirring, leading to the uniform growth of mesopores on 3D direction. The dendritic mesochannels with a "funneling" shape can be obtained by successive growth processes revolving round the nanoseeds. The process can be recycled many times on the interface, the 3D-dendritic MSNSs can be obtained by continuous growth, and the particle diameter can be continuously increased. Because of the limitation of the diameter of the oil@water hemimicelles, the silicate polymerization and cross-linking could not be continuously arisen on the "funneling" mesochannels of the nanoseeds along with the original gradient direction, therefore the new nuclei would emerge and subsequently the Y-type dendritic mesochannels can be formed. Finally, the uniform mesoporous silica spheres with dendritic and funneling mesochannels can be obtained.

The multigeneration hierarchical 3D-dendritic MSNSs can be obtained via continuous growth of the 3D-dendritic mesoporous channels on the surface of the first-generation products by changing the upper organic solution of the silicate source. The surface of the first-generation 3D-dendritic MSNSs can serve as a seed and core for further growth of the gradient dendritic mesochannels, because the nucleation concentration of the silicate oligomers on the heterogamous surface (solids) for the growth is much lower than the critical nucleation concentration. Furthermore, the preparation of Ag nanocube@3D-dendritic MSN and Au nanoparticle@3D-dendritic MSN core−shell composites can be realized. During the interfacial assembly process, the key factor for the mesopore size is the interfacial curvature of the surfactant/orgainic solvent/hydrophilic silicate emulsion, which is not only dependent on the molecular size and hydrophily/hydrophobicity of organic solvent, but also the amount of hydrophilic silicate source on interface. The emulsion occurs more easily and a larger curvature radius of hemiemulsion can be realized when the smaller molecular weight organic solvent such as cyclohexane is used as the upper oil phase, resulting in the formation of the larger pore 3D-dendritic mesoporous silica. When the high molecular weight organic solvent such as the decahydronaphthalene or 1-octadecene is used as an upper oil phase, the size of the hemiemulsion is smaller since the larger molecule size makes interfacial curvature to be smaller, leading to the formation of emulsion more difficult. Furthermore, when the concentration of the silica resource is lower, the pressure effect on the curvature radius is weaker with the fewer silicate oligomers around the hemiemulsion, resulting in the formation of larger diameter of the emulsion templates, and then large pore 3D-dendritic mesoporous silica spheres. Therefore, by changing TEOS concentration and up oil organic solvent, the hieratical pore size and multigeneration 3D dendritic MSNSs can easily be obtained.

In order to investigate whether the different pore sizes and generations can affect the loading and releasing in drug delivery system when the 3D-dendritic MSNSs are used as a protein nanocarrier, three kinds of the 3D-dendritic MSNS products with the same particle size but the different mesopore sizes and generations were designed and prepared. The first kind has a

dx.doi.org/10.1021/nl404316v | Nano Lett. 2014, 14, 923−932

pore size of ~5.5 nm (Figure 3a), and they are named as nanocarriers of 3D-dendritic MSNS-5.5; the second one has a pore size of ~10 nm (Figure 3b) as nanocarriers of 3D-dendritic MSNS-10; while the third one is two-generation 3D-dendritic MSNSs with a pore size of ~5.5 nm for the first generation and ~10 nm for the second generation (Figure 3c), named as 3D-dendritic MSNS-5.5@10. All three kinds of the protein nanocarriers have the same particle size of ~130 nm. The SAXS and BET data of these nanocarriers are shown in Figure 3d,e, providing the clear evidence to demonstrate the pore sizes and generations of them.

For the protein loading and releasing experiments, bovine β-lactoglobulin with the molecular size of 3.78 × 4.96 × 5.65 nm was chosen as a model protein. The isoelectric point (PI) of silanol on the surface of 3D-dendritic MSNSs is about 3.0, however, the PI value of the guest molecule bovine β-lactoglobulin is about 6.0. In protein loading measurements, the acetic acid-sodium acetate buffer (pH = 5.0) was used as the buffer, since the protein and nanocarriers (3D-dendritic MSNSs) can achieve the positive and negative charges, respectively. The 3D-dendritic MSNS-5.5 nanocarriers have the protein loading capacity of ~30.5 wt %, while the 3D-dendritic MSNS-10 with a larger mesopore size show a double loading capacity as 62.1 wt %, because the latter nanocarries have a double pore volume compared with the former. The two-generation 3D-dendritic MSNS-5.5@10 nanocarriers have the protein loading capacity of ~46.6 wt %, which is due to a little bit lower pore volume of the hierarchical mesostructure compared with the 3D-dendritic MSNS-10. For the protein releasing experiments in the Krebs solutions (pH = 7.4), the 3D-dendritic MSNSs and their guest molecules (proteins) can both have negative charges, therefore the electrostatic repulsive interaction not only can keep the nanocarriers dispersed but also provide the nanocarriers a driving force to release the guest proteins. The three nanocarriers resulted in different release curves (Figure 4a). The 3D-dendritic MSNS-5.5 nanocarriers with a small pore size show the extended release over more than 70 h, while the nanocarriers with a larger mesopore of ~10 nm reveal much quicker release and can be completed within 24 h. Interestingly, the two-generation 3D-dendritic MSNS-5.5@10 nanocarriers show a two-stage release, one in the first 2 h is similar to that for the 3D-dendritic MSNS-10 and another after 2 h is analogous to that of the 3D-dendritic MSNS-5.5. It suggests that the 3D-dendritic MSNS nanocarriers with multigeneration hierarchical mesostructure can lead to the multistage releasing of guest molecules.

It was found that when the 3D-dendritic MSNS nanocarriers were soaked in the simulated body fluid, the solution was gradually transformed from the milky white to a transparent liquid, while the protein was released out. The degradation of the 3D-dendritic MSNS-10 nanocarriers with a large mesopore size of 10 nm were tested as a model and tracked by TEM and SEM images, revealing a rapid degradation process completed in 24 h (Figure 4b–f and Supporting Information Figure S7). The whole degradation is a process from outside to inside. The 3D-dendritic MSNS-10 nanocarriers show the smooth surface before the degradation (Figure 4b and Supporting Information Figure S7a). The obvious defects can be clearly observed on the particle surface after the degradation for 4 h (Figure 4c). The particle size of the 3D-dendritic MSNS-10 nanocarriers is significantly decreased after 8 h (Figure 4d), while the surface of the nanospheres seemly become hairy due to the degradation (Supporting Information Figure S7b). With the increase of the degradation time, the mesopore frameworks of the 3D-dendritic MSNSs are gradually destroyed (Figure 4e and Supporting Information Figure S7c) and only some blurred fragments can be observed after 24 h (Figure 4f), indicating that the degradation is almost completed in this short period.

However, it takes much more time to degrade the nanocarriers with smaller pore sizes (3D-dendritic MSNS-5.5) indicated by the transformation of the solution from the milky white to a transparent liquid with the same degradation condition. The tracing TEM images reveal that for this nanocarrier with a smaller pore size of ~5.5 nm it takes almost 96 h to degrade undetectable small silicate fragment (Supporting Information Figure S9a–e), 4-fold time longer than that for the 3D-dendritic MSNS-10 with a larger pore of ~10 nm. The partial mesochannels in the 3D-dendritic MSNS-5.5 nanocarriers become larger and larger after the degradation for 12 h (Supporting Information Figure S9b), and some irregular cracks in the surface can be observed in the SEM images due to the irregular destruction of the mesostructure (Supporting Information Figure S9g). After 24 h, the particle size becomes much smaller, and some antenna-like pore wall fragments appear on the surface (Supporting Information Figure S9c). Seldom solid nanoparticles can be detected in the solution after 96 h, indicating almost complete degradation (Supporting Information Figure S9d,e).

^{29}Si MAS NMR spectra for the 3D-dendritic MSNSs exhibit two resonance bands at −100.8 and −110.2 ppm (Supporting Information Figure S6), which are characteristics of (HO)Si-$(OSi)_3$ (Q^3) and $Si(OSi)_4$ (Q^4) silicon species, respectively.[51] Via fitting the multipeaks by Gaussian method, the Q^3/Q^4 ratio for the 3D-dendritic MSNS-10 nanocarriers is calculated to be ~0.40, suggesting a low cross-liking degree of the silica frameworks. Meanwhile, the 3D-dendritic MSNS-5.5 nanocarriers with a small pore size (~5.5 nm) have an approximate Q^3/Q^4 ratio of ~0.46. It suggests that the 3D-dendritic MSNSs with different pore sizes have a similar low cross-linking silica framework.[51,52] It also provides the evidence that the degradation rate is mainly dependent on the pore size of the 3D-dendritic MSNSs.

Furthermore, the degradation of the two-generation 3D-dendritic MSNS-5.5@10 nanocarriers undergoes a two-stage process which can last about 72 h. The first stage is rapid degradation for the outside second-generation shells with a large pore size of ~10 nm. From the outside to inside, it is similar to the single-generation 3D-dendritic MSNS-10 nanocarriers. It takes about 12 h for the degradation of the pore channels of second-generation shells (Figure 4i). The nanoparticles lost their silica shells and seemly returns to the first generation (Figure 4g). Then the rest nanocarriers with a pore size of ~5.5 nm show a slow degradation rate in the following process (Figure 4j,k, Supporting Information Figure S8). The fragments of the silica nanoparticles can be rarely detected after 72 h (Figure 4l), indicating that the degradation is almost finished. All the results above suggest that the hierarchical mesostructure have a multistage hierarchical degradation behavior as a result of their unique structure.

It was reported previously that the free diffusion and charges auxiliary driving force were supposed to be the main factors for the protein releasing.[53] However, in our case for the 3D-dendritic MSNSs, the degradation probably played a more important role, because the guest molecules could be released into the solution with the silica gradual degradation process. Thus, multistage release can be achieved by the degradable

dx.doi.org/10.1021/nl404316v | Nano Lett. 2014, 14, 923–932

multigeneration hierarchical structures with controlled release rates.

Most importantly, the degradability of the 3D-dendritic MSNSs makes this kind of novel nanocarriers have a better biological compatibility compared with other conventional inorganic ones. Incubating HeLa cell with the 3D-dendritic MSNSs with the concentration from 0 to 10 mg/mL, there is not obvious difference for the cell viability (Supporting Information Figure S11). Even in a very high concentration (100 mg/mL of the 3D-dendritic MSNSs) for bioapplication, about 90% of cell viability also can be achieved for both 3D-dendritic MSNS-10 and 3D-dendritic MSNS-5.5 samples. For the extreme cytotoxicity, 1000 mg/mL of 3D-dendritic MSNSs was investigated, and cell viability of 3D-dendritic MSNS-10 and 3D-dendritic MSNS-5.5 was ∼47 and ∼37%, respectively, clearly demonstrating that these nanocarriers with faster biodegradation rate have less toxicity. On one hand, the low cross-linking degree of the mesoporous silica frameworks has the benefit in the degradation. On the other hand, large pore of the 3D-dendritic MSNSs favors the rapid degradation rate with the fast substance diffusion between the inside and outside. Their fast and tunable degradation rate is a unique advantage against other nanocarriers, while the some conventional features of mesoporous materials are still preserved.

In summary, a kind of novel 3D-dendritic mesoporous silica nanospheres with multigenerational and hierarchical dendrimer-like center-radial mesopore channels has been successfully synthesized via a new biphase stratification approach. The biphase stratification approach not only can control the uniform large pore size of the desired generations (three generation here) from ∼2.8 to 13 nm but also can tune the thickness of each generation for the mesoporous silica nanospheres from ∼5 to 180 nm. Furthermore, the biphase stratification approach also can be expanded to prepare uniform core−shell mesoporous structures with varied functional cores (such as Au nanoparticles and Ag nanocubes) and 3D-dendritic mesopores radial channels. The novel interfacial emulsion, "funneling" gradient assembly and growth mechanism is proposed, which undergoes a process including interfacial emulsion to form oil@water hemimicelles, exclusive composite micelles on the solid nuclei, "funneling" gradient assembly and growth of the mesostructures. The 3D-dendritic MSNSs reveal a fast degradability rate due to their large pore sizes and low cross-linking silica frameworks. The fastest degradation can be finished entirely in 24 h, which is greatly shorter than the two weeks of conventional mesoporous silica nanoparticles reported previously. With the remarked large pores and good degradability, this kind of 3D-dendritic MSNSs can be used as reliable protein nanocarriers and tunable protein releasing rates, which are demonstrated to be depended on the pore size. The larger mesopore size is, the faster degradability and releasing rates are. Furthermore, multigeneration 3D-dendritic MSNSs with different pore sizes and hierarchical mesostructure can realize the multistage degradation and guest molecule release. Thus, as a kind of novel biodegradable inorganic materials, the 3D-dendritic MSNSs are very useful for drug delivery, especially in the large-sized protein molecules. Moreover, it also can be used as supports for enzyme catalysis, pollutant enrichment, chromatography, and bioimaging and sensors.

■ ASSOCIATED CONTENT

Ⓢ Supporting Information

The experimental section, and the photo pictures of the reaction equipment and crystal films of the 3D-dendritic MSNSs; TEM, SEM images and ^{29}Si MAS NMR spectra of the 3D-dendritic MSNS products. This material is available free of charge via the Internet at http://pubs.acs.org.

■ AUTHOR INFORMATION

Corresponding Authors

*E-mail: (D.Z.) dyzhao@fudan.edu.cn.
*E-mail: (F.Z.) zhang_fan@fudan.edu.cn.

Author Contributions

⊥D.S. and J.Y. contributed equally to this work.

Notes

The authors declare no competing financial interest.

■ ACKNOWLEDGMENTS

The work was supported by the NSFC (21101029, 21273041, 21210004), China National Key Basic Research Program (973 Project) (2013CB934101, 2013CB934104, 2012CB224805, 2010CB933901), and China Postdoctoral Science Foundation (2013M531113).

■ REFERENCES

(1) Joo, S. H.; Park, J. Y.; Tsung, C. K.; Yamada, Y.; Yang, P.; Somorjai, G. A. *Nat. Mater.* **2009**, *8*, 126.
(2) Vallet-Regi, M.; Colilla, M.; Gonzalez, B. *Chem. Soc. Rev.* **2011**, *40*, 596.
(3) Hu, Y.; Zheng, X. T.; Chen, J. S.; Zhou, M. J.; Li, C. M.; Lou, X. W. *J. Mater. Chem.* **2011**, *21*, 8052.
(4) Tang, F.; Li, L.; Chen, D. *Adv. Mater.* **2012**, *24*, 1504.
(5) Wu, S. H.; Mou, C. Y.; Lin, H. P. *Chem. Soc. Rev.* **2013**.
(6) Zhou, Z.; Hartmann, M. *Chem. Soc. Rev.* **2013**, *42*, 3894.
(7) Huang, H. S.; Chang, K. H.; Suzuki, N.; Yamauchi, Y.; Hu, C. C.; Wu, K. C. W. *Small* **2013**, *9*, 2520.
(8) Chen, H.-W.; Chiang, Y. D.; Kung, C. W.; Sakai, N.; Ikegami, M.; Yamauchi, Y.; Wu, K. C. W.; Miyasaka, T.; Ho, K. C. *J. Power. Sources* **2014**, *245*, 411.
(9) Ashley, C. E.; Carnes, E. C.; Phillips, G. K.; Padilla, D.; Durfee, P. N.; Brown, P. A.; Hanna, T. N.; Liu, J.; Phillips, B.; Carter, M. B.; Carroll, N. J.; Jiang, X.; Dunphy, D. R.; Willman, C. L.; Petsev, D. N.; Evans, D. G.; Parikh, A. N.; Chackerian, B.; Wharton, W.; Peabody, D. S.; Brinker, C. J. *Nat. Mater.* **2011**, *10*, 389.
(10) Chen, Y.; Gao, Y.; Chen, H. R.; Zeng, D. P.; Li, Y. P.; Zheng, Y. Y.; Li, F. Q.; Ji, X. F.; Wang, X.; Chen, F.; He, Q. J.; Zhang, L. L.; Shi, J. L. *Adv. Funct. Mater.* **2012**, *22*, 1586.
(11) Tang, H. Y.; Shen, S.; Guo, J.; Chang, B. S.; Jiang, X. G.; Yang, W. L. *J. Mater. Chem.* **2012**, *22*, 16095.
(12) Pan, L.; He, Q.; Liu, J.; Chen, Y.; Ma, M.; Zhang, L.; Shi, J. *J. Am. Chem. Soc.* **2012**, *134*, 5722.
(13) Sun, Z. K.; Deng, Y. H.; Wei, J.; Gu, D.; Tu, B.; Zhao, D. Y. *Chem. Mater.* **2011**, *23*, 2176.
(14) Kim, M. H.; Na, H. K.; Kim, Y. K.; Ryoo, S. R.; Cho, H. S.; Lee, K. E.; Jeon, H.; Ryoo, R.; Min, D. H. *ACS Nano* **2011**, *5*, 3568.
(15) Huang, X. L.; Li, L. L.; Liu, T. L.; Hao, N. J.; Liu, H. Y.; Chen, D.; Tang, F. Q. *ACS Nano* **2011**, *5*, 5390.
(16) Gao, Y.; Chen, Y.; Ji, X.; He, X.; Yin, Q.; Zhang, Z.; Shi, J.; Li, Y. *ACS Nano* **2011**, *5* (12), 9788−9798.
(17) Zheng, H. Q.; Che, S. A. *RSC Adv.* **2012**, *2*, 4421.
(18) Kao, K. C.; Mou, C. Y. *Microporous Mesoporous Mater.* **2013**, *169*, 7.
(19) De Vocht, C.; Ranquin, A.; Willaert, R.; Van Ginderachter, J. A.; Vanhaecke, T.; Rogiers, V.; Versees, W.; Van Gelder, P.; Steyaert, J. *J. Controlled Release* **2009**, *137*, 246.

(20) Lobovkina, T.; Jacobson, G. B.; Gonzalez-Gonzalez, E.; Hickerson, R. P.; Leake, D.; Kaspar, R. L.; Contag, C. H.; Zare, R. N. *ACS Nano* **2011**, *5*, 9977.
(21) Vermonden, T.; Censi, R.; Hennink, W. E. *Chem. Rev.* **2012**, *112*, 2853.
(22) Mintzer, M. A.; Grinstaff, M. W. *Chem. Soc. Rev.* **2011**, *40*, 173.
(23) Lim, J.; Simanek, E. E. *Adv. Drug Delivery Rev.* **2012**, *64*, 826.
(24) Du, X.; Shi, B.; Liang, J.; Bi, J.; Dai, S.; Qiao, S. Z. *Adv. Mater.* **2013**, DOI: 10.1002/adma.201302189.
(25) Souris, J. S.; Lee, C. H.; Cheng, S. H.; Chen, C. T.; Yang, C. S.; Ho, J. A.; Mou, C. Y.; Lo, L. W. *Biomaterials* **2010**, *31*, 5564.
(26) Zhang, H. Y.; Dunphy, D. R.; Jiang, X. M.; Meng, H.; Sun, B. B.; Tarn, D.; Xue, M.; Wang, X.; Lin, S. J.; Ji, Z. X.; Li, R. B.; Garcia, F. L.; Yang, J.; Kirk, M. L.; Xia, T.; Zink, J. I.; Nel, A.; Brinker, C. J. *J. Am. Chem. Soc.* **2012**, *134*, 15790.
(27) Kaehr, B.; Townson, J. L.; Kalinich, R. M.; Awad, Y. H.; Swartzentruber, B. S.; Dunphy, D. R.; Brinker, C. J. *Proc. Natl. Acad. Sci. U.S.A.* **2012**, *109*, 17336.
(28) Chen, Y.; Chen, H. R.; Shi, J. L. *Adv. Mater.* **2013**, *25*, 3144.
(29) Tarn, D.; Ashley, C. E.; Xue, M.; Carnes, E. C.; Zink, J. I.; Brinker, C. J. *Acc. Chem. Res.* **2013**, DOI: 10.1021/ar3000986.
(30) Chu, P. K.; Chen, H. M.; Hu, T.; Zhang, X. M.; Huo, K. F.; He, J. H. *Langmuir* **2010**, *26*, 13556.
(31) Yamada, H.; Urata, C.; Aoyama, Y.; Osada, S.; Yamauchi, Y.; Kuroda, K. *Chem. Mater.* **2012**, *24*, 1462.
(32) Tang, F. Q.; Liu, T. L.; Li, L. L.; Teng, X.; Huang, X. L.; Liu, H. Y.; Chen, D.; Ren, J.; He, J. Q. *Biomaterials* **2011**, *32*, 1657.
(33) Wan, Y.; Zhao, D. *Chem. Rev.* **2007**, *107*, 2821.
(34) Kresge, C. T.; Leonowicz, M. E.; Roth, W. J.; Vartuli, J. C.; Beck, J. S. *Nature* **1992**, *359*, 710.
(35) Zhao, D.; Feng, J.; Huo, Q.; Melosh, N.; Fredrickson, G. H.; Chmelka, B. F.; Stucky, G. D. *Science* **1998**, *279*, 548.
(36) Yokoi, T.; Karouji, T.; Ohta, S.; Kondo, J. N.; Tatsumi, T. *Chem. Mater.* **2010**, *22*, 3900.
(37) Wan, Y.; Shi, Y.; Zhao, D. *Chem. Commun.* **2007**, 897.
(38) Lefevre, B.; Galarneau, A.; Iapichella, J.; Petitto, C.; Di Renzo, F.; Fajula, F.; Bayram-Hahn, Z.; Skudas, R.; Unger, K. *Chem. Mater.* **2005**, *17*, 601.
(39) Polshettiwar, V.; Cha, D.; Zhang, X. X.; Basset, J. M. *Angew. Chem., Int. Ed.* **2010**, *49*, 9652.
(40) O'Callaghan, J. M.; McNamara, H.; Copley, M. P.; Hanrahan, J. P.; Morris, M. A.; Steytler, D. C.; Heenan, R. K.; Holmes, J. D. *Langmuir* **2010**, *26*, 7725.
(41) Lettow, J. S.; Han, Y. J.; Schmidt-Winkel, P.; Yang, P. D.; Zhao, D. Y.; Stucky, G. D.; Ying, J. Y. *Langmuir* **2000**, *16*, 8291.
(42) Moon, D. S.; Lee, J. K. *Langmuir* **2012**, *28*, 12341.
(43) Du, X.; He, J. *Nanoscale* **2012**, *4*, 852.
(44) Yu, M.; Zhou, L.; Zhang, J.; Yuan, P.; Thorn, P.; Gu, W.; Yu, C. *J. Colloid Interface Sci.* **2012**, *376*, 67.
(45) Frens, G. *Nat. Phys. Sci.* **1973**, *241*, 20.
(46) Zhang, Q.; Cobley, C.; Au, L.; McKiernan, M.; Schwartz, A.; Wen, L. P.; Chen, J. Y.; Xia, Y. N. *ACS Appl. Mater. Interf.* **2009**, *1*, 2044.
(47) Yang, J. P.; Shen, D. K.; Zhou, L.; Li, W.; Li, X. M.; Yao, C.; Wang, R.; El-Toni, A. M.; Zhang, F.; Zhao, D. Y. *Chem. Mater.* **2013**, *25*, 3030.
(48) Moeller, K.; Kobler, J.; Bein, T. *Adv. Funct. Mater.* **2007**, *17*, 605.
(49) Qiao, Z. A.; Zhang, L.; Guo, M. Y.; Liu, Y. L.; Huo, Q. S. *Chem. Mater.* **2009**, *21*, 3823.
(50) Monnier, A.; Schuth, F.; Huo, Q.; Kumar, D.; Margolese, D.; Maxwell, R. S.; Stucky, G. D.; Krishnamurty, M.; Petroff, P.; Firouzi, A.; Janicke, M.; Chmelka, B. F. *Science* **1993**, *261*, 1299.
(51) Steel, A.; Carr, S. W.; Anderson, M. W. *Chem. Mater.* **1995**, *7*, 1829.
(52) Simonutti, R.; Comotti, A.; Bracco, S.; Sozzani, P. *Chem. Mater.* **2001**, *13*, 771.
(53) Yiu, H. H. P.; Wright, P. A. *J. Mater. Chem.* **2005**, *15*, 3690.